# Radar Imaging from a Distorted Array

B. D. STEINBERG

*Airborne Radar Branch*
*Radar Division*

October 13, 1981

DTIC
ELECTE
OCT 1   1981

A

81  10  1  005

| REPORT DOCUMENTATION PAGE | READ INSTRUCTIONS BEFORE COMPLETING FORM |
|---|---|

| 1. REPORT NUMBER | 2. GOVT ACCESSION NO. | 3. RECIPIENT'S CATALOG NUMBER |
|---|---|---|
| NRL Memorandum Report 4646 | AD-A104 803 | |

| 4. TITLE *(and Subtitle)* | 5. TYPE OF REPORT & PERIOD COVERED |
|---|---|
| RADAR IMAGING FROM A DISTORTED ARRAY | Interim report on a continuing NRL problem. |
| | 6. PERFORMING ORG. REPORT NUMBER |

| 7. AUTHOR(s) | 8. CONTRACT OR GRANT NUMBER(s) |
|---|---|
| B.D. Steinberg | |

| 9. PERFORMING ORGANIZATION NAME AND ADDRESS | 10. PROGRAM ELEMENT, PROJECT, TASK AREA & WORK UNIT NUMBERS |
|---|---|
| Naval Research Laboratory Washington, DC 20375 | 62712N; WF12100000; 53-0666-0 |

| 11. CONTROLLING OFFICE NAME AND ADDRESS | 12. REPORT DATE |
|---|---|
| Naval Air Systems Command Washington, DC 20360 | October 13, 1981 |
| | 13. NUMBER OF PAGES |
| | 23 |

| 14. MONITORING AGENCY NAME & ADDRESS*(if different from Controlling Office)* | 15. SECURITY CLASS. *(of this report)* |
|---|---|
| | UNCLASSIFIED |
| | 15a. DECLASSIFICATION/DOWNGRADING SCHEDULE |

16. DISTRIBUTION STATEMENT *(of this Report)*

Approved for public release; distribution unlimited.

17. DISTRIBUTION STATEMENT *(of the abstract entered in Block 20, if different from Report)*

18. SUPPLEMENTARY NOTES

19. KEY WORDS *(Continue on reverse side if necessary and identify by block number)*

High resolution
High angular resolution
Radar imaging
Distorted array

Adaptive beamforming
Adaptive array

20. ABSTRACT *(Continue on reverse side if necessary and identify by block number)*

High angular resolution radar imaging may be achieved with a large-aperture antenna even if the aperture is distorted, provided that adaptive signal processing compensates for the distortion. An algorithm for imaging ground-based targets is described and experimental results are given for a 3 cm wavelength demonstration system using a distorted 27 m, random, sparse array. The measured beamwidth of one mr conformed to theory, confirming the validity of the technique. Extension of the algorithm to accommodate isolated targets such as aircraft and ships also is discussed.
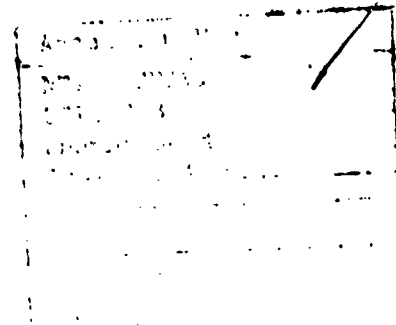
DD FORM 1473 EDITION OF 1 NOV 65 IS OBSOLETE
S/N 0102-014-6601

i

# TABLE OF CONTENTS

iii

# RADAR IMAGING FROM A DISTORTED ARRAY

## INTRODUCTION

A microwave array may be distorted for many reasons: It may be too large to be surveyed properly. It may suffer from windloading. Its installation may be faulty. Or its distortion may be electrical rather than geometric: Medium turbulence can cause the integral of the dielectric constant over a path from a source or a target to the array to vary randomly with position in the array. Electromagnetic coupling from the antenna elements to the local environment also may vary randomly with position in the array, causing random errors in the driving point impedances of the antenna elements. The tolerance on the random variation is about 30° rms or somewhat less than one-tenth wavelength [1].

That a microwave array designed for high angular resolution imaging is likely to suffer from one or more of these difficulties is evident from an examination of (1)

$$\hat{s}(u) = \int_L i(x)[\int s(u)e^{jkxu}du]e^{-jkx u}dx \qquad (1)$$

which is the simplest form of the integral equation relating a source function or scene s and its image or estimate $\hat{s}$ when the radiation field due to the source is measured by a line aperture of extent L having aperture weighting i. The source is assumed to be in the far field of the aperture, which permits its description in terms of the one-dimensional reduced angular variable $u = \sin\theta$, $\theta$ being measured from the normal to the aperture. The aperture also is assumed to be one-dimensional. The exponential kernels are Fourier kernels and both integrals are Fourier integrals. The inner integral is the radiation field S at the aperture. (1) can be written in terms of S:

$$\hat{s}(u) = \int_L i(x)S(x)e^{-jkxu}dx$$

$$= \mathcal{F}\{i(x)S(x)\} \qquad (2)$$

where $\mathcal{F}\{\cdot\}$ means Fourier transform. By the multiplication-convolution property of the Fourier transform

$$\hat{s}(u) = \mathcal{F}\{i(x)\} * \mathcal{F}\{S(x)\}$$

$$= I(u)*s(u) \qquad (3)$$

1

where * means convolution. I(u) is the radiation or diffraction pattern of the aperture. Since convolution broadens or spreads a function, the closer that I(u) approximates a δ-function, the better the estimate $\hat{s}(u)$ is of s(u). Since the width of I(u) is always the order of $\lambda/L$, it is evident that the larger the aperture size L the more closely will s be **represented** by $\hat{s}$. The same conclusion pertains to a target or scene in the near field.

To achieve a resolving power of $10^{-4}$ to $10^{-5}$ rad, which is typical of common optical instruments such as cameras and small telescopes, a microwave antenna must be hundreds of meters to tens of kilometers in size. Such antennas are too large to be constructed as single structures such as the parabolic dish. Instead they must be phased arrays. They must be highly thinned (mean interelement spacing >> $\lambda/2$) to control costs, and the element distribution must be aperiodic to eliminate grating lobes [1]. It is most likely that the large size will preclude accurate knowledge of element location; hence, the array properties will tend to degenerate to those of the random array and the system design must accomodate the poor sidelobe performance expected from such an array [2]. As a consequence, array distortion is a highly likely property of a huge array designed for microwave imaging. However, its effect can be neutralized to a considerable extent by adaptively controlled phase corrections within the system based upon measurements at the array of the radiation field from a point source [3,4]. Adaptive, retrodirective beamforming techniques then focus the distorted array upon the source [5,6].

The paper describes an algorithm for phase synchronizing or self-cohering a distorted array upon such a source, moving the focused beam in range and angle to a target area, and scanning it across the target to image it. An instrument embodying this procedure is called a radio camera. Experimental evidence of the validity of the technique is given. The experiments were conducted with an X-band ($\lambda = 3$ cm) radar, using a distorted, quasi-linear, random antenna array 27 m long.

THE RADIO CAMERA

Figure 1 shows a badly distorted receiving array and a point-source of radiation in its near field. It also shows a pulsed transmitter. The near-field source may be active, such as a beacon, or passive, such as a large cross-section reflector echoing the radiation from the transmitter. This source or reflector is called the adaptive beamformer; it also is called the phase synchronizer. The array is shown measuring the phase of the signal received at each element relative to the phase at some reference element within the array. In the absence of multipath the phase $\phi_n$ of the received signal at the nth element is $(\omega r_n/c_n) + \xi_n$, where $\omega$ is the radiation frequency $r_n$ is the path length, $c_n$ is the average speed of propagation over the path and $\xi_n$ is the phase shift through the receiving element and associated circuits. $\phi_n$ may be rewritten as

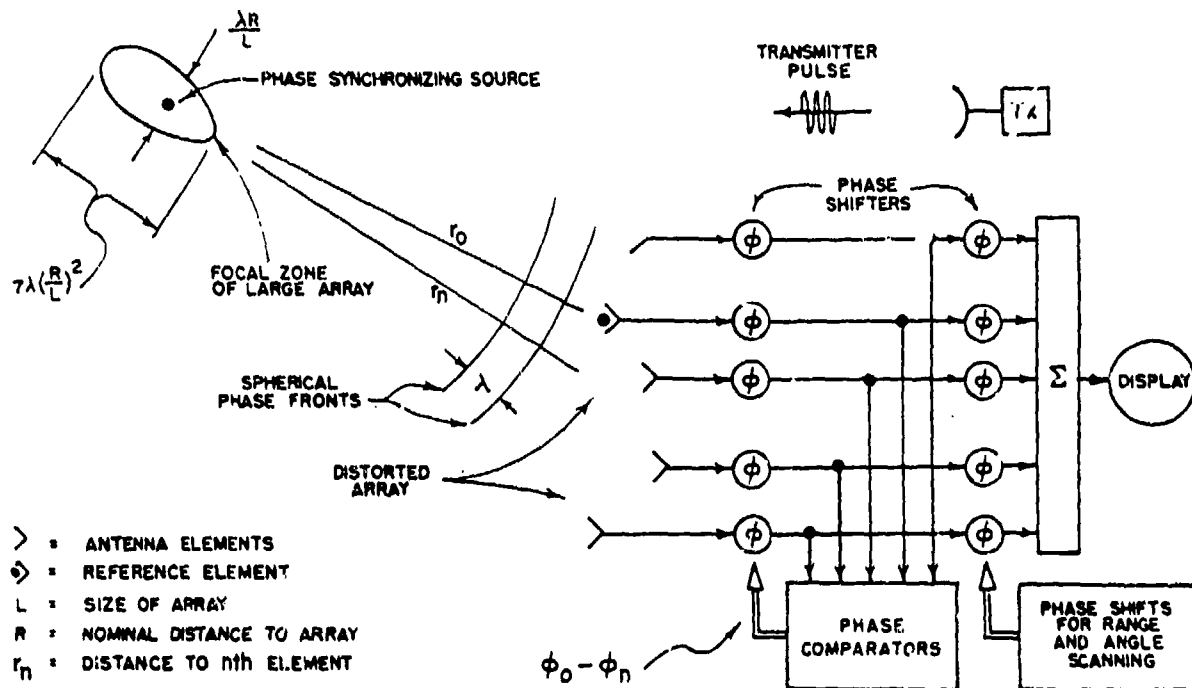$$\phi_n = \frac{\omega(r_{on} + \delta r_n)}{c_o + \delta c_n} + \xi_n \qquad (4)$$

2

Fig. 1 — Distorted array self-coheres on a phase synchronizing source

to explicitly show the displacement $\delta r_n$ of the element in the direction toward the adaptive beamformer from its correct distance $r_{on}$, and the deviation $\delta c_n$ of the mean propagation speed over the nth path from the average speed $c_o$ in the medium. Since $\delta c_n \ll c_o$,

$$\phi_n \approx \frac{\omega (r_{on} + \delta r_n)(1 - \delta c_n/c_o)}{c_o} + \xi_n$$

$$\approx kr_{on} + k\delta r_n - \frac{kr_{on}\delta c_n}{c_o} + \xi_n, \quad k = \frac{\omega}{c_o}$$

(5)

The phase differences from element to element are seen to have four components. The primary component $kr_{on}$ is due to source location relative to the undistorted array and is the same as in any phased array. The residuals are due to the distorted geometry of the array, to variations in propagation

3

conditions from the source to different parts of the array due to its large size, and to variations in electromagnetic coupling between the elements and their surroundings. By phase-shifting each receiver channel by the negative of these phase differences, all signals from the adaptive beamformer become cophased. The output, following summation, is that of an array focused upon the beamforming source. The spot size of the focal zone in the near field, calculated from diffraction theory, is shown in the figure. It is nominally $\lambda R/L$ in the cross-range dimension and $7\lambda(R/L)^2$ in range. $\lambda/L$ is the beamwidth of a focused diffraction-limited aperture of length L; it also is the beam-width of the distorted array following the adaptive beamforming procedure. $7\lambda(R/L)^2$ is the approximate value of the 3 dB range beamwidth due to the limited depth of field of an aperture focused on a near-field target [1]. $\lambda R/L$ also is the far-field cross-range dimension.

Also shown schematically in the figure is a second set of phase shifters located prior to the summer. Unlike the first phase shifting operation, the second operation is open loop and nonadaptive. After the array is phase syn-chronized the focused beam is scanned in range and angle by open-loop correc-tions calculated from the geometry. The calculations are made exactly as in a conventional phased array. During near-field scanning the spot size and shape remain as indicated in the figure. In the very near field the resolu-tion of the two-dimensional image that results from the scanning operation is about equal to the spot size. When the target is in the far field of the large array the depth of field becomes infinite and the resolution in range is determined by the pulse duration of the transmitter. At intermediate distances the range resolution is the smaller of the depth of field and the radar pulse length.

Both phase shift operations can be analog or digital. The phaselock loop is the natural analog circuit for adaptive beamforming. The experimental equipments described later use digital phase shifting. Figure 2 shows the procedure more explicitly. A transmitted pulse illuminates both a target area to be imaged and a passive phase synchronizing target, which is sketched as a corner reflector. The echo trace consists of their echoes plus clutter. The signals received at the several antenna elements are sampled in range and stored in the format shown. The range trace delivered by each antenna element is stored as a row of complex numbers. Successive rows correspond to succes-sive elements in the array. The position of a sample in a row is proportional to range and designates the range bin. The position of a sample in a column designates the array element number and is monotonic with but not necessarily proportional to element position since the array is distorted.

For simplicity it is assumed that $|r_n - r_m| \ll \Delta R$, all n, m, where $\Delta R$ is the length of a range cell. Thus, all echoes from a common target will appear in a single range bin in the format shown in Figure 2. Actually, target echoes can appear in different range bins for two reasons. The first is due to the large size of the array, for when $L \sin \theta > \Delta R$, the differential arrival time from a source at angle $\theta$ exceeds the pulse length. This effect is easily calculated and therefore may be corrected in the signal processor. The second cause is array distortion in the direction toward the source. Most arrays designed to be linear or planar systems will not suffer distortion so severe as to warrant range-bin correction, yet will still require adaptive phase cor-rection if the unknown a priori geometric distortion exceeds a small fraction
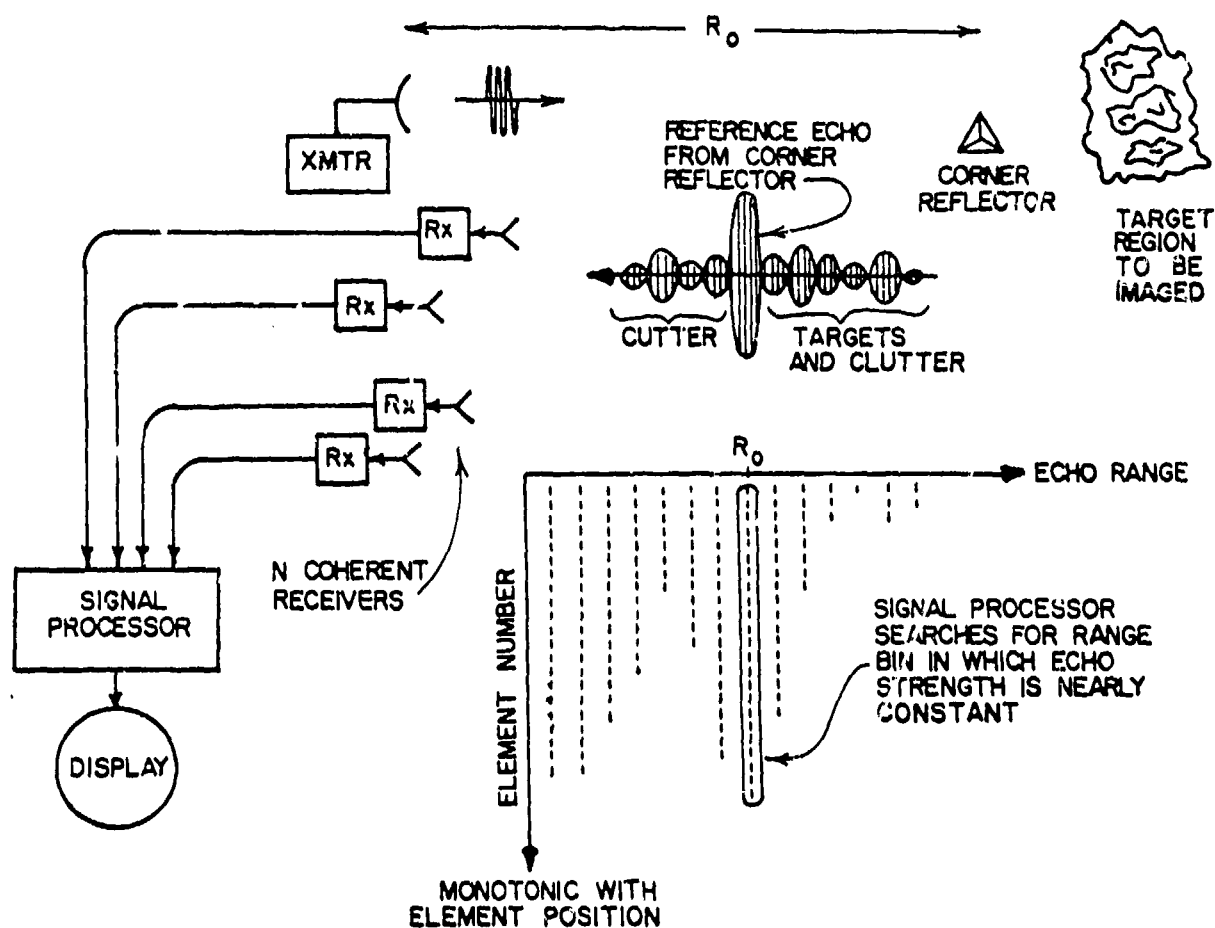
4

Fig. 2 — Radio camera data format and procedures

of a wavelength.  Large irregular arrays having deviations from planarity comparable to or exceeding $\Delta R$ also will require range-bin correction.

Assuming that range-bin correction, if needed, has been accomplished, three distinct additional operations upon the stored data are required for imaging.  These constitute the algorithm and are given in separate sections below.  Two are the beamforming and scanning operations discussed earlier. The third, which precedes these two, is the search procedure for the phase synchronizing source.

REFERENCE SIGNAL

The first operation of the signal processor following data sampling and storage is a search in range for a good phase synchronizing source, i.e., for that echo sequence across the array that most closely approximates the expected field from a point source. That range is designated $R_0$ and is the reference range, i.e., the range from which the phase synchronizing reference signal is obtained. The radiation field from a point source in free space would be nearly constant in amplitude across the array, while the phase differences would disclose the differential distances (modulo wavelength) to the source as well as the differential phase shifts through the receiving elements. A simple test to find that target whose radiation field most closely approximates that of a point source is to measure the normalized echo amplitude variance at each range. $R_0$ is that range for which the test value is minimum.

Figure 3 shows typical echo amplitude sequences measured across a large array. One is from a corner reflector and the other from a pick-up truck with camper top, which is a complicated target. The array was a 100 sample point, distorted aperture 27 m in length operating at 3 cm wavelength [3]. The corner reflector is the ideal adaptive beamformer, yet the echo amplitude pattern is not constant with element position. There are four contributing factors to the general variation of echo amplitude with element position. The first is due to the size of the reflector or source. The second is due to multipath. The third is due to clutter. The fourth is due to the radiation pattern of the antenna element used in the array.
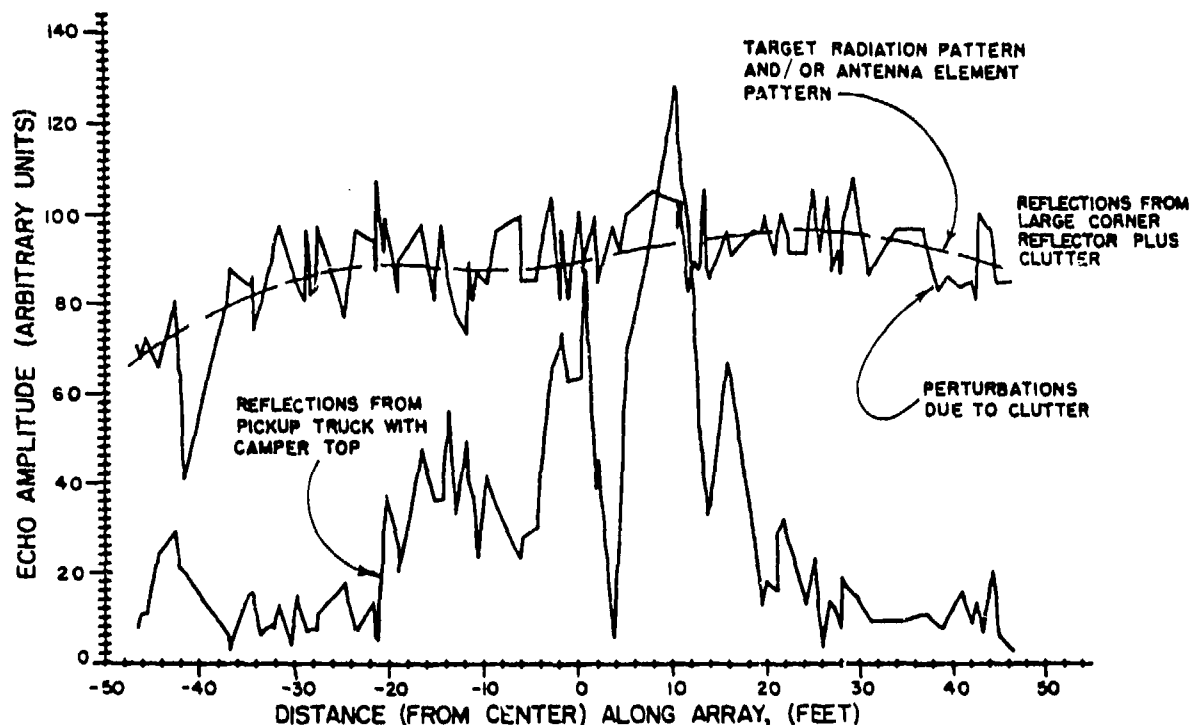


Fig. 3 — Echo strength from two range bins vs element position in array. The corner reflector approximates a point source.

6

A reflector of size T reradiates a lobular pattern in which the nominal lobe spacing is $\lambda/T$ rad (Figure 4, left). The nominal lobe spacing at the array, which is at a distance R, is $\lambda R/T$, and the echo sequence across the array would be expected to have a spatial period of this value. If $\lambda R/T \lesssim L$ a low spatial frequency or long period amplitude modulation would be evident in the measured data. Such a long period spatial modulation appears in the corner reflector echo sequence in Figure 3 (although the cause is not due to the size of the reflector but to the radiation pattern of the antenna element, which is discussed later).

The high spatial frequency or short period fluctuations seen in the corner reflector echo sequence in Figure 3 are due to clutter (Figure 4, middle). The transmitter beamwidth is broad compared to the high-resolution receiver beamwidth; the beamwidth $\Delta\theta = \lambda/a$, where a is the size of the radiating antenna. The clutter patch illuminated by the transmitter at distance R is $R\Delta\theta = R\lambda/a$. The lobes of the backscattered radiation have a nominal spacing $\lambda/(R\lambda a) = a/R$, and the nominal cross section at the array is equal to $R(a/R) = a$. This last expression means that the correlation distance of the spatial amplitude modulation due to the clutter equals the size of the transmitting antenna, which, in this experiment, was less than the average interelement distance. Since the transmitting antenna is small compared to the large receiving array, the clutter modulation always will appear, as in Figure 3, as a high spatial frequency or short period fluctuation.

The effect of multipath is similar. Let $\beta$ be the angular separation at the array between the direct arrival and the multipath signal. The complex amplitude of the received signal along the array (x coordinate) has the form $1 + \alpha\exp(jkx\beta)$ where $\alpha$ is the reflection coefficient of the multipath scatterer and $k = 2\pi/\lambda$ is the wavenumber. The period of the amplitude modulation of the sum of the two signals is $\lambda/\beta$. Rarely is $\beta > \Delta\theta$; therefore, multipath in general will introduce a lower spatial frequency into the echo sequence across the array.

The fourth contributing factor to the nonconstancy of the reference echo sequence is the radiation pattern of the receiving element used in the array. Figure 5 pictures four array elements each of length d in an array of length L. The beamwidth of an element pattern is $\lambda/d$ and its cross section at the beamforming target is $\lambda R/d$. The figure illustrates that when $L > \lambda R/d$ the element gain to the target varies with element position in the array.

The echo variance calculation should be based upon the first, second and third factors, which measure the quality of the radiation field for adaptive beamforming, but not the fourth factor, in which the measuring instrument induces a variation. The effect of the latter is minimized by dividing $V_{in}$, the echo amplitude from the ith range bin received by the nth element, by the estimated element pattern gain $\hat{f}_n$ from the nth element to the target.

(A single subscript suffices for the element pattern gain unless the target is in near field of the element, which is highly unlikely.)
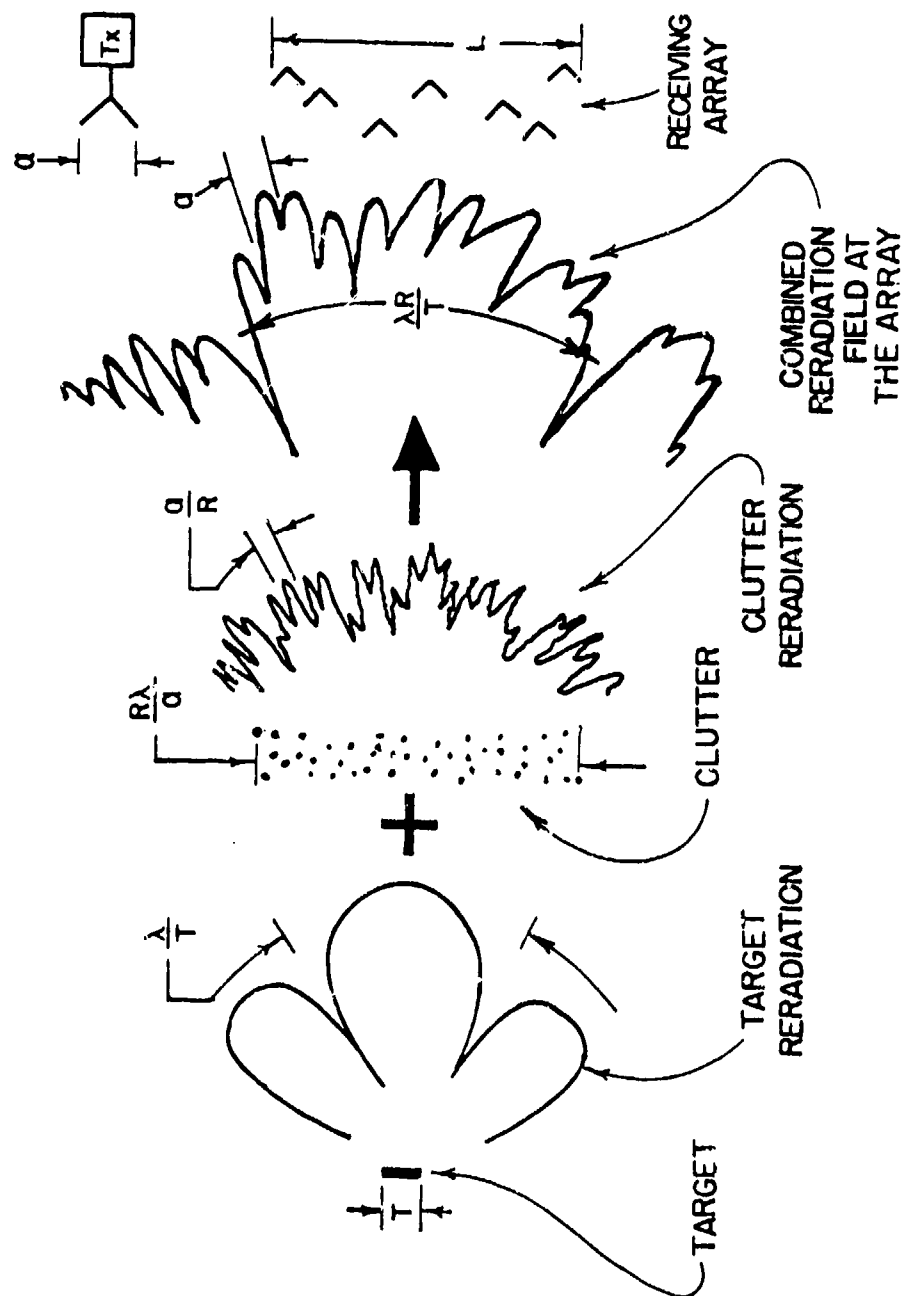
Fig. 4 — Target size and clutter contribute to echo amplitude variation across array

The corrected amplitude is

$A_{in} = V_{in}/\hat{f}_n$. Its mean $\overline{A_i} = \frac{1}{N} \sum\limits_{n=1}^{N} A_{in}$ and mean square $\overline{A_i^2} = \frac{1}{N} \sum\limits_{n=1}^{N} A_{in}^2$

are calculated, where N is the number of antenna elements. Its variance

$\sigma_i^2 = \frac{1}{N} \sum\limits_{n=1}^{N} (A_{in} - \overline{A_i})^2 = \overline{A_i^2} - \overline{A_i}^2$. $\sigma_i^2$ is normalized to $\overline{A_i^2}$ to remove the

effect of target strength and range from the calculations. The normalized

variance is $1 - \overline{A_i}^2 / \overline{A_i^2}$, which is a minimum at that range element for which

$\overline{A_i}^2 / \overline{A_i^2}$ is the largest value. The rule for finding $R_o$, then, is to calculate

$\overline{A_i}^2 / \overline{A_i^2}$ for all range elements and search for the largest value. The signal

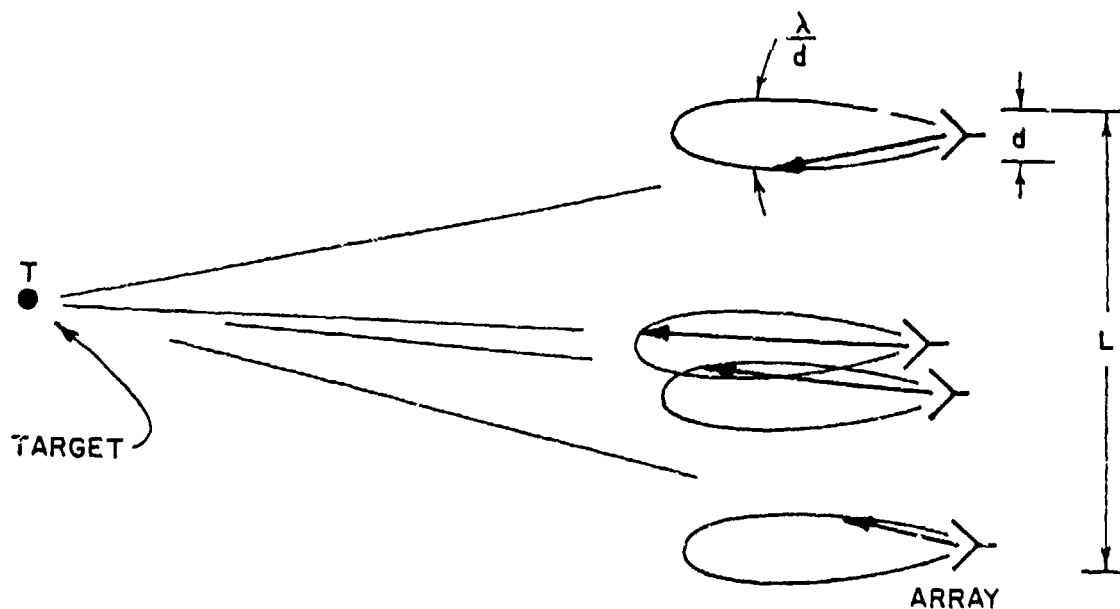sequence from that range bin becomes the reference signal.



Fig. 5 — The element pattern also contributes to amplitude variation

9

ADAPTIVE BEAMFORMING

Table 1 shows all the steps in the procedure. Step 1 initiates the process. $V_{in} \exp(j\psi_{in})$ is the complex envelope of the echo from the ith range bin received by the nth element. Steps 2 and 3 are the search for $R_0$ discussed above. Step 4 is the adaptive beamforming step. The measured phases $\psi_{in}$ can be broken into the sum of two terms $\psi'_{in} + \psi''_{in}$ . The first term contains the conventional target and array geometry and is all that would be expected in the absence of array distortion, medium turbulence, multipath and scattering. The second term represents the errors which the phase synchronization process must overcome. In the absence of such errors the image of the target or clutter from the ith range element would be obtained from the integral of the phase-weighted signals received across the array from the ith range bin. As in any phased array the phase weighting is the conjugate of the kernel of the diffraction integral. For ease of discussion the diffraction integral can be approximated by the Fresnel integral, which reduces to the Fourier integral when the target is in the far field. That integral in turn is best represented by a sum as in (6) because the array is discrete. The sum

$$\hat{s}_i(u) \approx \sum_{n=1}^{N} A_{in} e^{j\psi'_{in}} e^{-jk(x_n u - x_n^2/2R_i)} \tag{6}$$

is the image $\hat{s}_i$ of the scattering sources in the ith range bin provided that $\psi'' = 0$. As in (1), $u = \sin\theta$ and $\theta =$ scan angle from the normal to the array. The discrete variables $x_n$ and $R_i$ are, respectively, the x coordinate in the array (transverse to the array normal) of the nth element and the distance to the ith range bin. Although $\hat{s}_i(u)$ is written as a one-dimensional image (in the reduced angular variable u) of the echoes from the ith bin, it is, in reality, a two-dimensional image in u and R. Consequently, two-dimensional imagery is available for display of near-field targets.


The function of the adaptive processor is to compensate for $\psi''_{in}$ so that the operation described by (6) may be accomplished. The earlier steps in the process searched the data to find the range bin in which the echo amplitude across the array had the smallest variation. That range bin became the reference range and the signal from that range bin became the synchronizing signal. Its complex envelope following normalization to $\hat{f}$ is $A_{on} \exp(j\psi_{on})$ where the amplitudes are all nearly the same. The phases of the echoes are random, however, due to the perturbed geometry of the array or the spatial variations of the refractive index or the impedance variations from element to element or any combination of these factors. If the reference source were an ideal source the phase differences would be due entirely to them. In addition the phases are perturbed by multipath and scattering and by the finite lobe width of the reradiation from the synchronizing source. However, because it is generally impossible for the system designer to obtain a priori information about these latter conditions, the signal processor must necessarily ignore them.

The fourth step in the process is to compensate for the phase variations, which are assumed to be due to the first set of factors. Correction is accomplished by phase rotating the complex envelopes of the signals from $R_0$ received

by the different array elements. The proper phase shift for the nth element is the negative of the phase difference $\Delta\psi_{on} = \psi_{on} - \psi_{oo}$. The complex signal envelope at the nth element becomes $A_{on}\exp(j\psi_{on})\exp[-j(\psi_{on} - \psi_{oo})] \simeq A\exp(j\psi_{oo})$. This correction, or phase conjugation, is exactly what a phased array or lens would do when focusing upon the reference source. The output signal from the array when it is so focused is the sum of these phase-corrected echoes from $R_o$.

Table 1 — Steps in Radio Camera Imaging

| Step | | |
|------|---|---|
| 1 | Measure and store complex envelopes of echo samples | $V_{in}\,e^{j\psi_{in}}$ <br> range bin—↗↖—element number |
| 2 | Correct amplitudes by dividing by element pattern estimate $\hat{f}_n$ | $A_{in}e^{j\psi_{in}}$ |
| 3 | Find $R_o$ such that $f_{on} \simeq A$, all n | $Ae^{j\psi_{on}}$ |
| 4 | Phase conjugate at $R_o$ | $Ae^{j\psi_{oo}}$ |
| 5 | Phase rotate at all range elements | $A_{in}e^{j(\psi_{in} - \psi_{on} + \psi_{oo})}$ |
| 6 | Focus at each range $R_1$ | $A_{in}e^{j\left[\psi_{in} - \psi_{on} + \psi_{oo} + \frac{kx_n^2}{2}\left(\frac{1}{R_1} - \frac{1}{R_o}\right)\right]} \triangleq B_{in}$ |
| 7 | Phase shift linearly with angle | $B_{in}e^{-jkx_nu}$ |
| 8 | Sum at each range element | $\hat{s}_i(u) = \sum_{n=1}^{n} B_{in}e^{-jkx_nu}$ |

## SCANNING

The fifth step (performed simultaneously with Step 4) is to phase rotate all the signal samples from each antenna element by $\psi_{on} - \psi_{oo}$. The samples of the complex envelope from the ith range bin now become $A_{in}\exp[j(\psi_{in} - \psi_{on} + \psi_{oo})]$. The sum of such a set of complex samples represents the output of a misfocused phased array or lens since $\psi_{in} \neq \psi_{on}$ except at the range $R_o$ of the reference reflector.

The sixth step is to focus the array at all ranges simultaneously. This task is accomplished for an arbitrary range $R_i$ by refocusing the array from the reference range $R_o$ to $R_i$. The phase correction is approximately quadratic, as given by (6). Assuming that the earlier steps were performed properly, the self-cohering process forced the quadratic component of the phase shift of the signal in the nth channel to become $-kx_n^2/2R_i + kx_n^2/2R_o$. To focus the array to range $R_i$ this term must be set to zero, which requires a further phase addition of $(kx_n^2/2)(1/R_i - 1/R_o)$. This step requires a knowledge of the range $R_o$ of the reference reflector. Fortunately, the value of $R_o$ is available in the system for it is measured, as in conventional radar, by the round-trip travel time of the pulse to the phase synchronizing source and it is read directly into the signal processor from the radar receiver. The accuracy of measurement is determined by the range resolution of the system, which is the order of the reciprocal of the signal bandwidth (in distance units), or the near-field range beamwidth, whichever is smaller.

Step 7 imparts a linear phase rotation to the range-focused complex envelope (designated $B_{in}$ in Table 1) for each scan angle u. The phase shift is $-kx_nu$.

The last step forms the sum of the linearly phase-weighted, range-focused samples to obtain the image $\hat{s}_i(u)$ for the ith range bin:

$$\hat{s}_i(u) = \sum_{n=1}^{N} B_{in}e^{-jkx_nu} \qquad (7)$$

## ELEMENT POSITION TOLERANCE

Steps 3, 4, and 5 require no knowledge whatsoever of element position. The phase synchronization process is purely retrodirective. Steps 6 (refocusing in range) and 7 (scanning in angle) do require coordinate information. The tolerances on element position error have been worked out [7], [8], [1, Chapter 13]. The most stringent tolerance is invoked by Step 7. Briefly, the theory consists of the following points. First, the loss in main lobe gain, in dB, due to all the random phase errors across the array is $\Delta G \approx 4.3\sigma_\phi^2$ where $\sigma_\phi^2$ is the variance of the phase errors in square radians. Second, the phase variance due to random position errors is approximately $\sigma_\phi^2 \approx k^2\sigma_x^2\theta^2$ where $\sigma_x^2$ is the position error variance in the array in the direction perpendicular to the beamforming direction and $\theta$ is the scan angle measured from the direction of beamforming.

12

Combining these expressions, and allowing one dB loss in array gain as an acceptable gain-loss tolerance, the rms element tolerance becomes

$$\sigma_x \approx \frac{\lambda}{4\pi} \theta_{max}^{-1} .$$

The factor $\lambda/4\pi$ is the conventional tolerance in phased array, mirror or lens design. $\theta_{max}$(rad) is the maximum scan angle from the direction of the reference source and is half the field of view. Since an individual radar target always subtends a very small angle at the radar, $\theta_{max} \ll 1$ and the allowed element position error is exceedingly large. For example, if the system were designed to image a target as large (in angle) as the moon, $\theta_{max}$ would be approximately $10^{-2}$ rad; in this case the position accuracy tolerance increases by two orders of magnitude to about $10\lambda$. It is precisely this extraordinary liberty in position tolerance, following adaptive phase synchronization, that permits radio camera imaging with a nonrigid or ill-surveyed array.

EXPERIMENTS

Figure 6 shows the result of an X-band radio camera imaging experiment using a low power (5w) pulsed radar transmitter and a corner reflector for the phase synchronizer. The size of the reflector was 0.46m and its radar cross-section was calculated to be $56m^2$. The estimated clutter cross-section was $2m^2$. The receiving array was the one use in the experiment for Figure 3; it was 27m long and 1.2m wide. The 100 element positions were randomly located within it. Uniform probability density functions of element position were chosen for both the length and width dimensions of the array. The experiment was conducted on a time-shared basis in which a single radar receiver was successively moved from position to position, delivering a radar echo trace to a microprocessor from each radar position, after which the operations described earlier were performed. The image is one-dimensional, deflection modulated. The target consisted of two additional reflectors, each 0.61m, drawn to scale below the image. Target distance from the array was 240m. The reference reflector was 41m closer. Drawn also in Figure 6 is the calculated response of the array in free space had it self-organized perfectly. It is evident that the experiment was exceedingly successful.

The theoretical beamwidth for this experiment, based upon diffraction theory, was $0.88\lambda/L\cos\theta$. The coefficient corresponds to the particular probability density function of element location used [1]. $\theta$, the target angle from the array normal, was 25°. This expression evaluates to 1.1mrad, which is indistinguishable from the measured beamwidth.

Figure 7 is the image of the same reflectors when the equipment was operated in the synthetic aperture mode [9]: the low power transmitter and receiver both were moved from position to position for each radar transmission and reception. (The experimental set and procedure were illustrated and described in [3].) Because of the doubling of the wavenumber due to the synthetic aperture operation, the beam cross-section in Figure 7 is halved. Again, the comparison with the calculated free space response is excellent.

In both experiments the sidelobe properties conform to the theory of the random array [1,2], which predicts that the contribution to the average
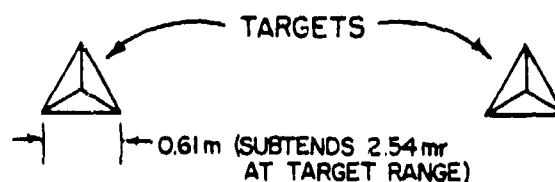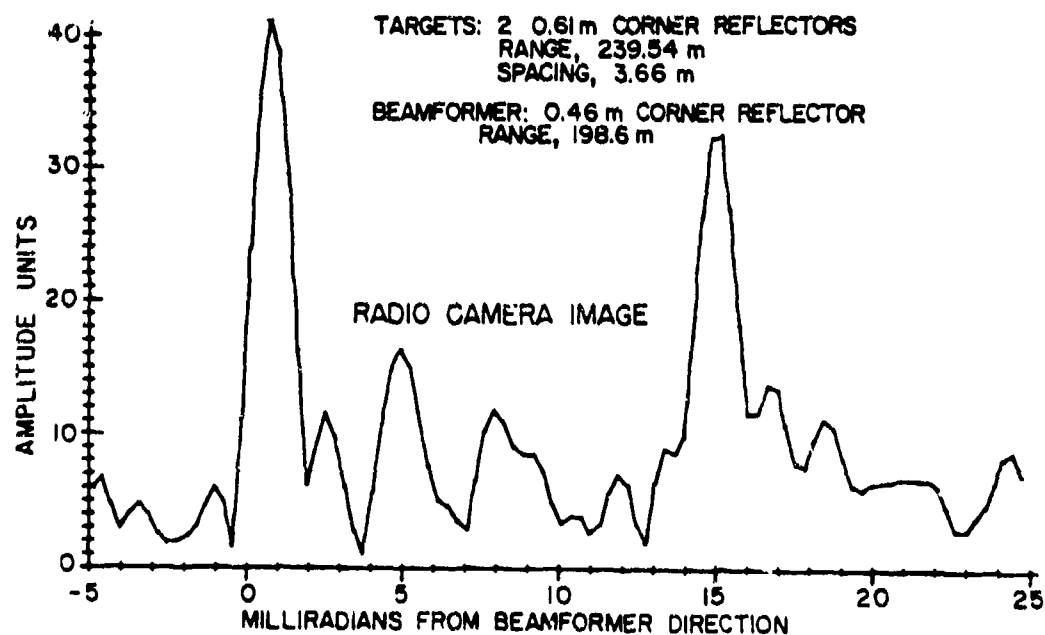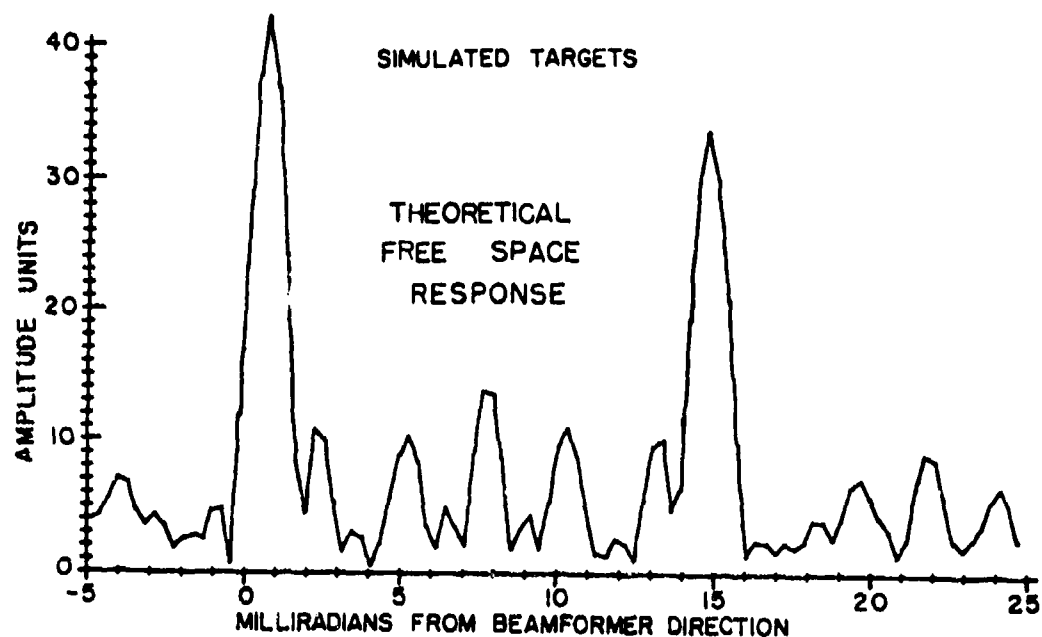
13

Fig. 6 — One-dimensional image of two corner-reflector targets using another corner reflector for adaptive beamforming. Theoretical response in free space shown for comparison.
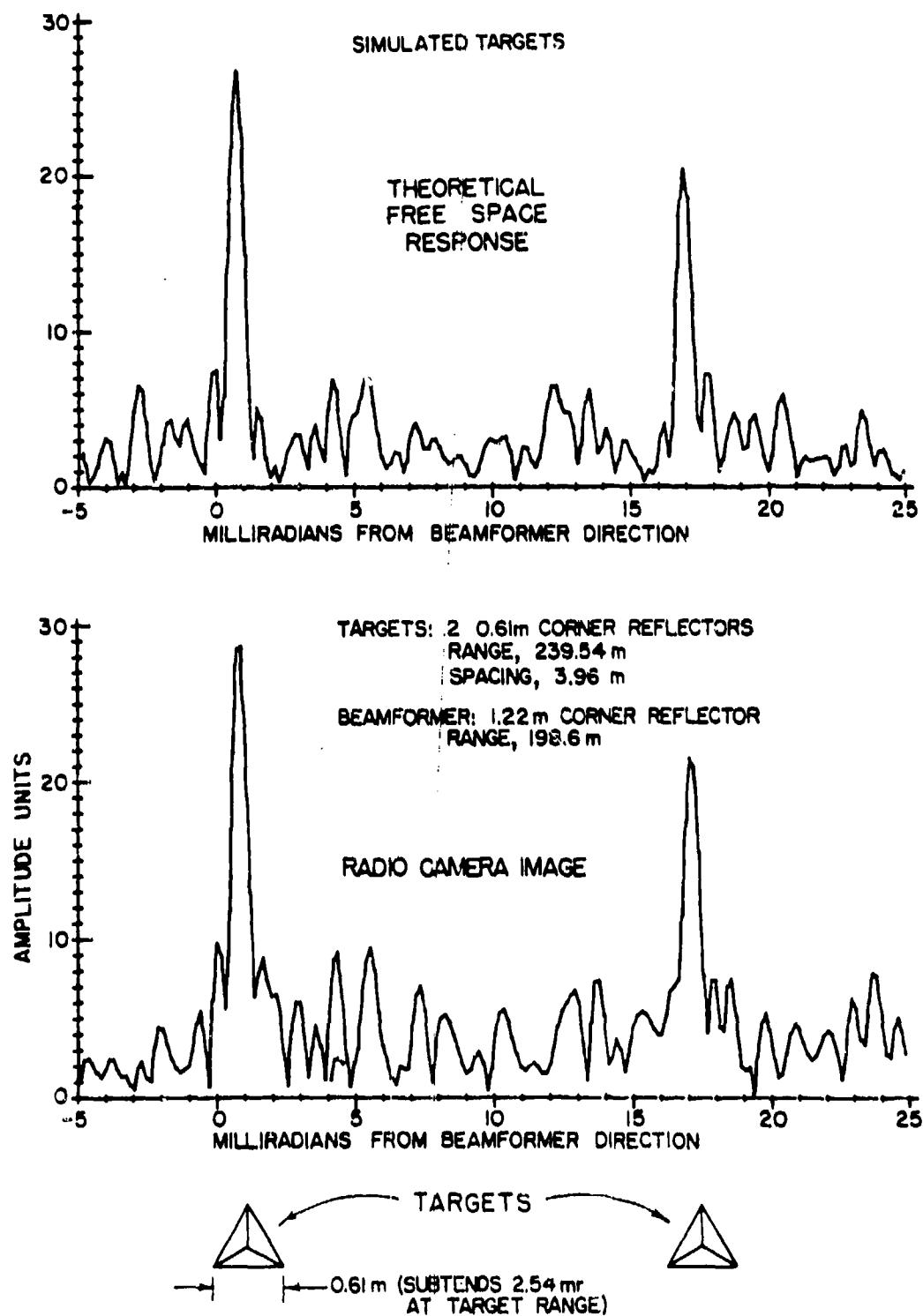
14

Fig. 7 — Radio camera image of same two targets in synthetic aperture mode

sidelobe power level is $N^{-1}$ times the main lobe power response of a target. Thus, the theoretical average sidelobe level for the two nearly equal strength targets in Figures 6 and 7 is -17 dB; the measured levels are within a few tenths of a decibel of this value.

## ISOLATED TARGET

The situation is somewhat different for an isolated target such as an aircraft or a ship in which the reference source is on the target. One difference is that no range refocusing (Step 6 of Table 1) is required since the size of the aircraft usually will be small compared to the depth of field of the array. A more significant difference lies in the fact that target echoes are used both for adaptive phase synchronization as well as for imaging. The requirements upon the echo characteristics are opposed for these two processes. Phase synchronization requires a dominant point source, whereas the objective of picture taking is to reproduce the angular backscatter profile of a complicated target so that it may be recognized.

The conflict resolves itself when the target is moving relative to the observer. Figure 8 shows an aircraft at distance R with its velocity vector V making an angle $\alpha$ with the direction to the array. The aspect angle $\alpha$ changes with time at the rate $d\alpha/dt = V \sin\alpha/R$. Because of this turning motion, the radar echo changes with time, sometimes having the desirable properties for phase synchronization while at other times the return signal is good for imaging purposes. From time to time a strong highlight appears due, say, to a broadside specular return from the fuselage, or a two-plane corner reflector formed by wing and fuselage or in the tail assembly. The highlights are severely aspect-angle dependent, as is demonstrated in Figure 9. There a small flat-late reflector of length T is shown momentarily oriented broadside to the direction to the array. As the line-of-sight angle $\theta$ changes due to platform motion the reradiation pattern moves through twice that angle. Consequently, the time that the main lobe dwells upon the array is determined by the turning rate $d\alpha/dt$ and the reradiation beamwidth ($\approx \lambda/T$). The duration or correlation time can be estimated as the time required for the differential phase of the echoes from two scatterers separated a distance equal to the target size T to change about $\pi/2$. The right of Figure 9 shows the geometry. The change in the differential distance $\delta R$ from two such scatterers is approximately $Td\alpha$. The rate of change is $d(\delta R)/dt \approx Td\alpha/dt = TV \sin\alpha/R$ and the phase difference between their echoes changes at a rate $i(\delta\phi)/dt = 2kd(\delta R)dt \approx 4\pi TV \sin\alpha/\lambda R$. Hence, the correlation time is the order of

$$T_c \approx \lambda R/8TV \sin\alpha \qquad (8)$$

Consider a Mach 1 aircraft with a reflecting region one meter in size oriented normal to the radar line-of-sight. When observed with 3 cm radiation from a distance of 20 km and at a 30° angle the correlation time is about 1/2 s. During this time the large array on the ground may be synchronized, forming a narrow beam focused on the specular reflector. Rather than determining at what range to phase conjugate or focus, as in the earlier discussion (Step 3 of Table 1), the signal processor now determines when to perform this operation. Its criterion is exactly the same, i.e., reasonable uniformity of echo strength across the array. Furthermore, it can apply an additional and highly sensitive
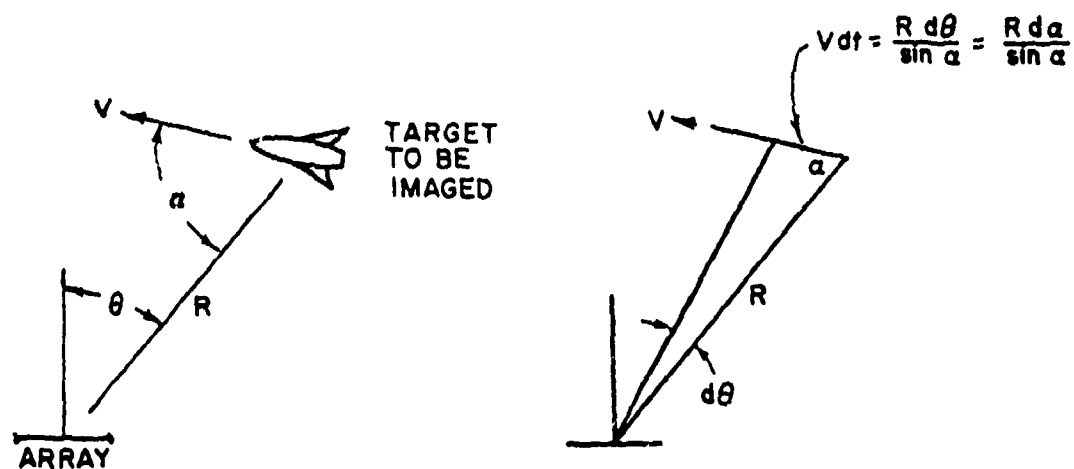
16

$$Vdt = \frac{R\,d\theta}{\sin\alpha} = \frac{R\,d\alpha}{\sin\alpha}$$

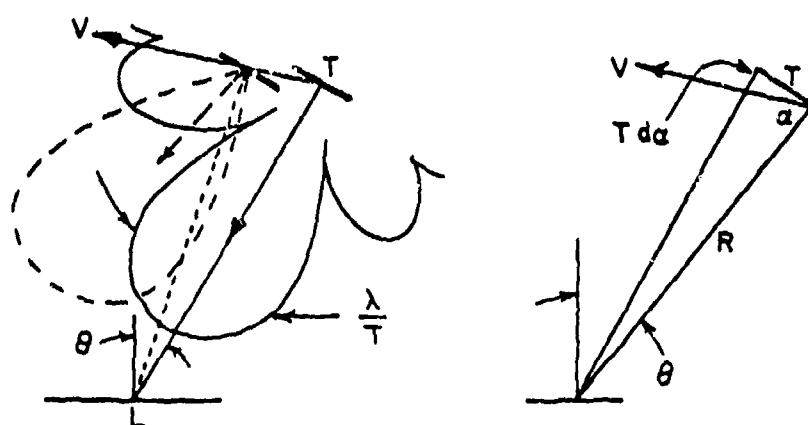Fig. 8 — The aspect angle $\alpha$ with time

Fig. 9 — The reradiation pattern rotates with platform motion

17

measure: The correlation time, which is the reciprocal of the echo modulation bandwidth, varies inversely with target size. When the highlight disappears the "target" in (8) becomes the size of the aircraft. If the one meter flat plate reflector were on a 30 m aircraft the modulation rate would jump by a factor of 30 following the 1/2 s phase synchronizing period. Similarly, the echo modulation bandwidth would drop by this factor when a stable echo appears, thereby permitting the signal processor to readily determine when to phase synchronize.

Observation of the drop in echo modulation bandwidth can be made in the low-frequency control branch of the phaselock loop, if such a circuit is used for adaptive beamforming, or in the data store of a real-time digital processor. In the latter case the data may be organized in the same format shown in the lower part of Figure 2 except that the horizontal coordinate is no longer range, but time. All the data come from the same range bin and the columns are spaced by one interpulse period. Successive columns are successive range-gated samples of the echoes at each antenna element. The processor observes the data bandwidth and the amplitude stability to determine when to phase synchronize (Step 3). During the dwell time of a highlight the signal processor ceases the imaging process and phase conjugates instead (Step 4). Next it observes when the modulation bandwidth returns to normal, at which time it begins again the imaging process (Steps 7 and 8). Following the high-resolution angle scan it awaits the next synchronizing interval to repeat the process. The cycle time is the order of one second. During several such seconds the aircraft has moved and rotated insignificantly insofar as the observer is concerned, but has altered its orientation sufficiently to cause successive images to be statistically independent. Hence, the logical next step is to form "multiple exposures," i.e., sums of intensities of several successive images. Doing so builds up the information content in the image and fills in the speckles or glint resulting from the narrowband (near monochromatic) radiation. In addition, it reduces the sidelobe peaks of the random array by several dB [1].

An experiment has been conducted to measure highlight dwell times and the percentages of time that aircraft targets are in the so-called "synchronizing" and "imaging" modes [10]. The basis for the measurement is the expected change in the probability density function (pdf) of the echo amplitude when a highlight occurs. Without it the echo is the vector sum of a large number of small, randomly phased echoes. The sum is a two-dimensional, zero mean, random Gaussian variate, the amplitude of which is Rayleigh distributed, i.e., if A is the echo amplitude and $2\sigma^2$ is its mean square value, the pdf of A is

$$f(A) = (A/\sigma^2)\exp(-A^2/2\sigma^2).$$

When a strong scatterer of strength $A_o$ is added, the pdf changes to the Ricean distribution

$$f(A) = (A/\sigma^2)\exp[-(A^2+A_o^2)/2\sigma^2]I_o(AA_o, \sigma^2),$$

where $I_o$ is the modified Bessel function of the first kind and zeroth order (which reduces to the Rayleigh pdf when $A_o = 0$) [11].

The experiment was designed to gather simple statistics on the short-time pdfs of radar echoes from aircraft. The radar was an L-band AN/TPS-1D. It is located at the Valley Forge Research Center of the Moore School of Electrical

18

Engineering, University of Pennsylvania, at Valley Forge, Pennsylvania, 40 km west of Philadelphia. Commercial aircraft flying in the Philadelphia-New York-Scranton triangle were observed and tracked. Distances varied from 15 to 100 km. Echo sequences of varying numbers of pulses were sorted by amplitude in real time in a histogram generator and the nature of the pdf was judged to be Rayleigh, Ricean or nondescript.

The results are shown in the tables below for broadside, nose and tail aspect. Sample histograms are shown in Figure 10. As expected, Rayleigh and Ricean pdfs did occur, the former with about three times the frequency of the latter (Table 2). About 20% of the sample runs showed no preference for either, exhibiting instead tendencies toward uniformity or bimodality, for example. The average correlation time in each mode also was measured (Table 3). Note that the 1/2 s dwell time estimated earlier for the sync mode is within the range shown. The measurements confirmed the expectation that aircraft will alternately permit array synchronizing and imaging.
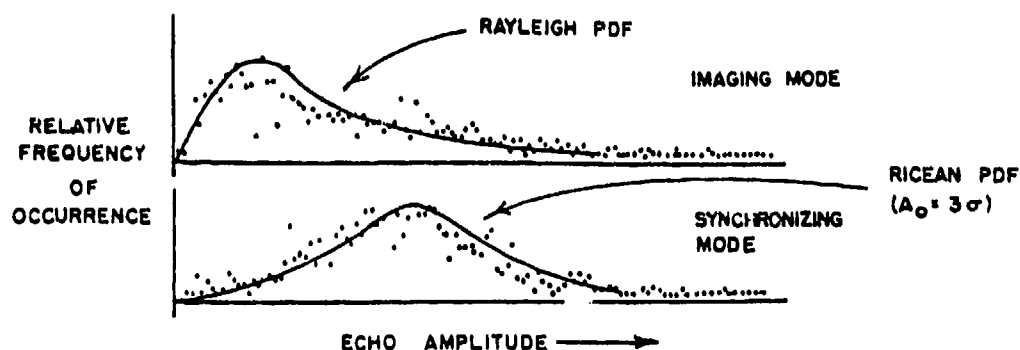


Fig. 10 — Histograms of aircraft echo sequences

Table 2 — Relative Frequencies of Occurrence of the Imaging and the Phase Synchronizing Modes

| View | Number of Aircraft | Imaging Mode (Rayleigh pdf) | Synchronizing Mode (Ricean pdf) | Neither |
|---|---|---|---|---|
| Broadside | 3 | .594 | .286 | .120 |
| Nose | 2 | .501 | .363 | .136 |
| Tail | 4 | .668 | .048 | .284 |
| All | 9 | .606 | .193 | .201 |

Table 3 — Approximate Correlation Times for Aircraft Echos

| View | Number of Aircraft Observed | Average Correlation Time(seconds) | Average Deviation (seconds) |
|------|------|------|------|
| Broadside | 16 | 1.56 | 0.68 |
| Nose | 7 | 0.30 | 0.04 |
| Tail | 4 | 0.17 | 0.11 |

SUMMARY

A radar antenna array distorted beyond the normal tolerance of about one-tenth wavelength can be made to function as a diffraction-limited imaging aperture by adaptively phase-compensating for the distortion. An external point source of radiation, called the phase synchronizer or adaptive beamformer, illuminates the array. The source may be an active beacon or a passive reflector echoing the radiation from a radar transmitter. The phase of the radiation field is measured at each array element. Phase shifts are added to each element channel to eliminate the phase differences. An array focused at the beamforming source results. Open loop scanning in range and angle follow adaptive focusing of the array.

An algorithm suitable for digital signal processing is given. It describes (1) a search procedure for locating the target most favorable for adaptive beamforming, (2) the adaptive beamforming process and (3) range and angle scanning of the focused beam.

Experimental evidence of the validity of the technique is given, based upon experiments with a 27 m, X-band, random, sparse array.

A modification to the basic algorithm is described to accomodate an isolated target such as an aircraft or a ship. A radar experiment with aircraft of opportunity disclosed that the fluctuating properties of airborne target echoes satisfy the requirements of the search procedure for a suitable adaptive beamforming source.

ACKNOWLEDGEMENTS

REFERENCES

[1]   Bernard D. Steinberg, Principles of Aperture and Array System Design,
      John Wiley and Sons, New York, 1976.

[2]   Y. T. Lo, "A Mathematical Theory of Antenna Arrays with Randomly Spaced
      Elements," IRE Trans. Antennas Propag., AP-12, May 1964, pp. 257-268.

[3]   Bernard D. Steinberg, Earl N. Powers, Donald Carlson, Bernard Meagher,
      Jr., Raymond S. Berkowitz, C. Nelson Dorny, Sam H. Seeleman, "First
      Experimental Results from the Valley Forge Radio Camera Program,"
      Proc. IEEE Letters, Vol. 67, No. 9, September 1979, pp 1370-1371.

[4]   Bernard D. Steinberg, "High Angular Microwave Resolution from Distorted
      Arrays," Proc. 1980 International Computing Conference, Vol. 231,
      April 1980, pp. 150-156.

[5]   The special issue on Active and Adaptive Antennas of IEEE Trans.
      Antennas Propag., AP-12, No. 2, March 1964, contains 13 papers on
      retrodirectivity.

[6]   R. C. Hansen (ed.), Microwave Scanning Antennas, V L. 3, Academic Press,
      New York, 1964.  See Chapter 5 by D. L. Margerum.

[7]   Bernard D. Steinberg, "Design Approach for a High-Resolutio Microwave
      Imaging Radio Camera," Journal of the Franklin Institute, Vol. 296,
      No. 6, December 1973, 415-432.

[8]   S. Hassan Taheri and Bernard D. Steinberg, "Tolerances in Self-Cohering
      Antenna Arrays of Arbitrary Geometry," IEEE Trans. Antennas Propag.,
      Vol. AP-24, No. 5, September 1976, 733-739.

[9]   Raymond S. Berkowitz and Earl N. Powers, "Tasar, A Thinned Adaptive
      Synthetic Aperture Radar," IEEE EASCON '78 Record, Arlington, VA,
      IEEE Publication 78 CH 1354-4 AES, 135-142.

[10]  Donald L. Carlson, "The Phase Synchronization of Large Random Arrays
      Using Specular Aircraft Radar Return Signals," M.S. Thesis, University
      of Pennsylvania, Philadelphia, PA, 1975.

[11]  S. O. Rice, "Mathematical Analysis of Random Noise," Bell System
      Technical Journal, No. 23, July 1944, pp. 282-332, No. 24, January 1945,
      pp. 46-156.

21